JOURNAL OF GEOPHYSICAL RESEARCH, VOL. 99, NO. D7, PAGES 14,429–14,441, JULY 20, 1994

Radiative-convective model with an explicit hydrologic cycle 1. Formulation and sensitivity to model parameters

Nilton O. Rennó,[1] Kerry A. Emanuel, and Peter H. Stone
Center for Meteorology and Physical Oceanography, Massachusetts Institute of Technology, Cambridge

Abstract. A hydrological cycle is explicitly included in a one-dimensional radiative-convective equilibrium model which is coupled to a "swamp" surface and tested with various cumulus convection schemes: the hard and soft convective adjustment schemes, the Kuo scheme, the Goddard Institute for Space Studies (GISS) (1974) model 1 scheme, the GISS (1983) model 2 scheme, and the Emanuel scheme. The essential difference between our model and other radiative-convective models is that in our model the moisture profile (but not cloudiness) is interactively computed by the cumulus convection scheme. This has a crucial influence on the computation of the radiative fluxes throughout the atmosphere and therefore on the model's sensitivities. Using the Emanuel scheme, we show that the climate equilibrium is very sensitive to cloud microphysical processes. Clouds with high precipitation efficiency produce cold and dry climates. Clouds with low precipitation efficiency lead to moist and warm climates. Since climate equilibrium can be very sensitive to the cloud microphysical processes, any cumulus convection scheme adequate for use in general circulation models (GCMs) should be strongly based on them. The cumulus convection schemes currently in use in GCMs bypass the microphysical processes by making arbitrary moistening assumptions. We suggest that they are inadequate for climate change studies.

1. Introduction

One-dimensional radiative-convective models are very useful for understanding the heat budget of planetary atmospheres. Their main value is that they allow one to examine general principles and to test fundamental ideas. Their major drawback is the inability to compute the feedbacks between the horizontal heat transports and the temperature structure from first principles. Also, in the literature, they usually lack the ice-albedo–temperature feedback, although the latter has been successfully included in a radiative-convective model by *Wang and Stone* [1980]. In spite of the inability of these one-dimensional models to compute the horizontal transports, multidimensional models (e.g., general circulation models (GCMs)) are not yet clearly superior for studying global climate change. This is apparent from the large errors in GCM simulations of atmospheric transports, which are very sensitive to the sub-grid-scale physics [*Stone and Risbey*, 1990]. It is also apparent from the large artificial sources of heat and moisture that coupled atmosphere-ocean GCMs need to simulate the current climate [*Manabe et al.*, 1991].

Radiative-convective models have been widely employed to simulate the thermodynamic structure of the atmosphere of Earth and other planets as well as its sensitivity to an increase in CO_2 content or changes in the flux of incoming solar radiation [*Manabe and Strickler*, 1964; *Manabe and Wetherald*, 1967; *Manabe*, 1971; *Sarachik*, 1978; *Lindzen et al.*, 1982]. Similar models also have been used to study the equilibrium solutions of the convective boundary layer over the tropical oceans [*Betts and Ridgway*, 1988, 1989] as well as its sensitivity to increases in CO_2 content.

Lindzen et al. [1982] explored the sensitivity of radiative-convective models to the choice of the cumulus convection parameterization scheme when calculating the climate consequences of changes in the solar forcing or of the atmosphere's CO_2 content. However, their cumulus convection parameterization schemes did not explicitly compute the vertical distribution of water vapor. Instead, the vertical distribution was diagnosed assuming a fixed climatological profile of relative humidity [*Manabe and Wetherald*, 1967]. Although this is a common practice in climate studies with one-dimensional radiative-convective equilibrium models and is approximately consistent with observations of seasonal change, this assumption lacks a rigorous physical basis.

Sarachik [1978] used a very simple radiative-convective model, coupled to a one-dimensional ocean model, to explore the sensitivity of the equilibrium sea surface temperature to changes in the solar constant. He concluded that the tropical sea surface temperature is relatively insensitive to changes in the solar constant and pointed out that additional solar flux is compensated mainly by additional evaporation. However, Sarachik did not account accurately for the warming effect of increased atmospheric water vapor transported by convective motions forced by the increased evaporation. He used a simple Newtonian cooling law to compute the atmospheric radiative cooling and an empirical formula to compute the downward longwave radiation at the ocean surface. Furthermore, he assumed a constant Bowen ratio to

[1]Now at Lawrence Livermore National Laboratory, Livermore, California.

Paper number 94JD00020.
0148-0227/94/94JD-00020$05.00

compute the sensible heat flux from the surface and considered the atmosphere's mixed layer to be always in equilibrium (meaning that the heating by the surface's sensible heat flux is equal to the cooling of the mixed layer by radiation). Sarachik's model fails to account for water vapor feedback and the possible decrease in the cooling of the planetary boundary layer due to an increase in the free atmosphere's water vapor content.

Betts and Ridgway [1988, 1989] used a radiative-convective model to study the sensitivity of the tropical convective boundary layer to various physical parameters. In their model the water vapor distribution is computed through a mixing line assumption [*Betts*, 1982, 1985] with parameters chosen to result in computed water vapor profiles similar to climatological profiles. This representation is very close to an assumption of constant relative humidity. Furthermore, Betts and Ridgway specified an arbitrary heat transport by the ocean to force the heat budget to be close to observed values.

The main drawback of the previous climate studies with radiative-convective models is the fact that they did not include the hydrological cycle, instead, the atmosphere's water vapor mixing ratio was diagnosed based on the climatological profile of relative humidity [*Manabe and Strickler*, 1964; *Sarachik*, 1978; *Lindzen et al.*, 1982]. The exception to this rule is the model of *Betts and Ridgway* [1988] in which the water vapor vertical distribution was computed through a mixing line assumption [*Betts*, 1982, 1985], but here too the water vapor profile is severely constrained by climatology. Thus, in general, previous models used very simple numerical procedures to parameterize cumulus convection. Since water vapor is the most important greenhouse gas [*Lindzen*, 1990] and its content and vertical distribution in the atmosphere is to a large extent controlled by moist convection, it is desirable to explicitly compute the atmospheric water vapor content. In the present work we explicitly include a hydrological cycle in a one-dimensional radiative-convective equilibrium model. [*Rennó*, 1992]. Furthermore, in this model, cumulus convection is parameterized by a variety of complex schemes, similar to those used in GCMs. The following cumulus convection parameterization schemes are compared: the moist convective adjustment scheme [*Manabe et al.*, 1965], the Kuo scheme [*Kuo*, 1974], the Goddard Institute for Space Studies (GISS) model 1 scheme [*Arakawa*, 1969; *Somerville et al.*, 1974], hereafter referred to as the GISS1 scheme, the GISS model 2 scheme [*Hansen et al.*, 1983], hereafter referred to as the GISS2 scheme, and the Emanuel scheme [*Emanuel*, 1991]. We use two versions of the moist convective adjustment scheme: one is in the form originally proposed by *Manabe et al.* [1965], hereafter referred to as the hard convective adjustment (HCA) scheme, while the other is the soft convective adjustment scheme (SCA). In this scheme it is assumed that only a fraction of the convecting grid is covered by convection.

We employ some of the most widely used schemes in our analysis. Of the 18 GCMs intercompared by *Cess et al.* [1990], 6 use MCA schemes. The Atmosphere Modeling Intercomparison Project (AMIP) [*Gates*, 1992] study shows that out of 29 GCMs, 9 use Kuo schemes, 8 use the MCA scheme, 8 use the Arakawa-Shubert scheme, 2 use the Tiedtke scheme, and 1 uses the Bougeault, the Hack, the GISS2, and the Gregory schemes. The Hack scheme is very similar to the GISS2 scheme. It is evident that the Kuo, the MCA, and the Arakawa-Shubert schemes are the most widely used in GCMs.

The purpose of this paper is to present the formulation of a one-dimensional radiative-convective model and to explore its sensitivity, with the various cumulus convection schemes, to the model's arbitrary parameters, and to the cloud's microphysical processes. We believe that an understanding of these sensitivities is essential for the interpretation of model results.

Our results show that a good understanding of the essential physics governing the water vapor transport by cumulus convection is crucial in climate simulations. Part 2 will explore the sensitivities to large changes in the solar forcing and the breakdown of the radiative-convective equilibrium, i.e., the runaway greenhouse. Part 3 will explore the sensitivities of the radiative-convective equilibria to CO_2 doubling and to small changes in the solar forcing.

2. Description of the Model

2.1. Model Equations

The model's basic equations are

$$\frac{\partial \theta}{\partial t} = Q + R + F_\theta, \tag{1}$$

$$\frac{\partial r}{\partial t} = C + F_r. \tag{2}$$

Independent variables are time, t, and pressure, p. The prognostic variables are the potential temperature, θ, and the water vapor mixing ratio, r. Q in (1) represents the diabatic heating by cumulus convection and large-scale condensation and C in (2) stands for the moisture source. These terms are computed by the cumulus convection scheme and represent the net effects of cumulus convection. R in (1) represents the net radiative heating. Radiation is computed by a parameterization scheme [*Chou*, 1992; *Chou et al.*, 1991], described in section 2.3.

Vertical diffusion of potential temperature and moisture are represented, respectively, as

$$F_\theta = g \frac{\partial \tau_\theta}{\partial p}, \tag{3}$$

$$F_r = g \frac{\partial \tau_r}{\partial p}, \tag{4}$$

where the variable τ_θ represents the vertical flux of potential temperature and τ_r represents the vertical flux of water vapor. In the free atmosphere they are estimated as

$$\tau_\theta = \rho^2 g k_{v\theta} \frac{\partial \theta}{\partial p}, \tag{5}$$

$$\tau_r = \rho^2 g k_{vr} \frac{\partial r}{\partial p}, \tag{6}$$

where $k_{v\theta}$ and k_{vr} are vertical diffusion coefficients for each variable, ρ is the air density, and g is gravitational acceleration. We present results of experiments with values of diffusion coefficients generally equal to 2 m^2 s^{-1}. This small diffusion is not supposed to represent any real physical

process but is added to stabilize the integrations. In the cloud layer, the observed eddies are represented by the parameterized convection.

We use centered differences in the vertical direction. Time integration of the nondiffusive terms is performed using a leapfrog scheme with an *Asselin* [1972] filter inserted at every time step to damp its computational mode. The smoothing constant of the Asselin filter is set at 0.1. The time integration of the diffusive terms is performed using the Euler forward scheme. The time step is set to 15 min and radiative fluxes are computed each 12 hours. Cumulus convection and large-scale condensation are computed every time step. Experiments are made with the number of vertical layers equal to 16 in the model's troposphere. The thickness of these vertical layers is constant in pressure. The troposphere's top is at 40 mbar and the model's surface is at 1000 mbar. Above the model's troposphere there is an upper layer extending from 40 to 1 mbar in radiative equilibrium. This upper layer is subdivided into 10 sublayers for the computation of the radiative fluxes.

2.2. Boundary Conditions

Since the main role of the ocean in radiative-convective equilibrium is to provide a surface boundary condition (we are only interested in the equilibrium), we use a "swamp" as the lower boundary. The swamp is a saturated surface in which the heat capacity is zero and the supply of moisture is infinite. Therefore the net energy flux into the surface is required to be zero at each instant. This is not exactly true in our model, since for numerical stability we set the swamp temperature equal to the averaged temperature computed in the last 96 time steps (24 hours).

Surface fluxes are computed with the bulk aerodynamic formulae

$$\tau_0 = \rho_a C_D |\mathbf{v}_a| (\theta_s - \theta_a), \tag{7}$$

$$\tau_r = \rho_a C_D |\mathbf{v}_a| (r_s - r_a), \tag{8}$$

where the subscript s refers to values at the surface and the subscript a refers to values at a level just above the surface, the anemometer level. C_D is a drag coefficient, set equal to 0.0025; $\mathbf{v}_a$ is the wind speed at the anemometer level, 5 ms^{-1}; θ_s is the surface potential temperature computed by the swamp formulation; r_s is the water vapor mixing ratio at the surface and it is the saturation mixing ratio of the surface; θ_a and r_a are the potential temperature and water vapor mixing ratio, respectively, at the anemometer level. They are computed on the basis of temperature and water vapor mixing ratio at the model's lowest level. The potential temperature and the water vapor mixing ratio are made constant from the model's lowest level down to the surface. The surface pressure, p_s, is fixed at 1000 mbar. The upper boundary is in a condition of radiative equilibrium and the water vapor mixing ratio above 40 mbar is set to values from the Air Force Geophysical Laboratory (AFGL) standard atmosphere [*McClatchey et al.*, 1972].

2.3. Radiation Model

We use a fast radiation parameterization scheme developed by *Chou et al.* [1991] and *Chou* [1992]. The scheme uses several broadband parameterizations for longwave and shortwave radiation in combination to produce a computationally fast and accurate representation of radiation.

For longwave absorption, *Chou*'s [1984] broadband transmission approach for water vapor, *Chou and Peng*'s [1983] for carbon dioxide, and the *Chou and Kouvaris* [1986] method for ozone are used. These approaches rely on parameterizations of gas-diffuse transmittance functions, appropriately weighted by the Planck blackbody source terms. These schemes include the water vapor line and continuum absorption, carbon dioxide absorption through band centers and band wing regions, and infrared ozone-absorption bands. The curve fitting was done with a Planck function evaluated from 160 to 330 K. Therefore the scheme works well for temperatures up to 330 K, but the errors tend to grow unpredictably above this temperature.

Solar radiation is absorbed by water vapor and ozone and reflected at the surface. The scheme employs the parameterization method of *Chou* [1992] for ozone and water vapor. By this method a five-term exponential-sum infrared transmission function models the near-infrared water vapor bands. Two albedo values, 1.0 for visible wavelengths and 0.99 for near-infrared wavelengths, are used to approximate the spectral dependence of the droplet single-scattering albedo. The Rayleigh scattering and cloud reflection are treated using a two-stream method for a range of conditions varying from cloudy sky of arbitrary optical depth to clear sky.

The reference carbon dioxide concentration (330 ppm), ozone mixing ratio, and stratospheric water vapor profile are from the AFGL standard atmosphere [*McClatchey et al.*, 1972].

2.4. Cumulus Convection Schemes

2.4.1. Hard convective adjustment (HCA). The main assumption in the HCA scheme is that when the lapse rate of a saturated area exceeds the moist adiabatic lapse rate, free convection within the explicit cloud is strong enough to maintain a constant profile of equivalent potential temperature, θ_e. The equivalent potential temperature of the adjusted layers, $\theta_{e_{\mathrm{adj}}}$, is computed by an iterative process to keep the vertically integrated moist static energy, $C_p T + L_v r + gz$, invariant during the convective adjustment. The adjusted layers are kept saturated and the excess water vapor falls out as rain without reevaporation. If any layer is supersaturated and its temperature lapse rate does not exceed the moist adiabatic, then large-scale condensation occurs. After large-scale condensation the layer is kept just saturated, while its temperature is increased by the release of latent heat of condensation. This scheme was implemented following *Manabe et al.* [1965].

2.4.2. Soft convective adjustment (SCA). The soft convective adjustment scheme is similar to the HCA scheme, except for the fact that the saturation requirement for convection to occur is relaxed and that the moist adjustment occurs over a specified fraction of the grid-scale area. Over the remaining area the vertical profiles of temperature and humidity remain constant. Therefore when moist convection occurs, the adjustment is computed at each level by the equations

$$\partial T^k = (T^k_{\mathrm{adj}} - T^k_{\mathrm{env}})(1 - \sigma), \tag{9}$$

$$\partial r^k = [r_{\mathrm{sat}}(p^k, T^k_{\mathrm{adj}}) - r^k_{\mathrm{env}}](1 - \sigma), \tag{10}$$

where T is the absolute temperature, r is the water vapor mixing ratio, and σ is an arbitrary parameter that can be

adjusted empirically. The superscript k refers to each of the n unstable layers, while the subscripts adj and env refer to the cloud and environment variables, respectively. We use $\sigma = 0.037$, because for this value of σ, the agreement between observed and computed precipitation was best in experiments performed by *Krishnamurti et al.* [1980]. Everything else is computed as in the HCA scheme.

Moist convective adjustment schemes should be thought of as a representation of turbulence within clouds, rather than representations of the clouds themselves. In practice, some grid points will contain such clouds and others will not; to represent the collective effect of ensembles of clouds, it is necessary to have both cloudy and clear grid points. Running convective adjustment schemes in strictly one-dimensional mode invariably results in saturation. To more realistically represent an ensemble of clouds, we actually simulate the clear air surrounding the cloud and assume that the clouds cover very small fractional areas. To simulate the water vapor content of the air outside of clouds, we calculate the amount of air rising (the convective mass flux) in the saturated column (the convective cloud) as that required by the convective heating, i.e., the convective mass flux that is just enough to balance the condensation heating inside the convective clouds with adiabatic cooling. Then, the environment is adiabatically warmed by the compensating subsidence forced by moist convection. The amount of water vapor in the cloud free region is the result of downward advection of dry air by the forced subsidence and of detrainment of saturated cloud air.

The compensating subsidence mass flux forced by moist convection is given by

$$M_c = -\frac{1}{g}\left(\frac{\partial\theta}{\partial p}\right)^{-1}\left(\frac{\partial\theta}{\partial t}\right)_c, \tag{11}$$

where M_c is defined as positive when it is downward. The subscript c refers to moist convection values.

The convective moistening is computed as follows:

$$\frac{\partial r}{\partial t} = -M_c\frac{\partial r}{\partial p} + \alpha(r_c - r)\frac{\partial M_c}{\partial p} \quad \text{if } \frac{\partial M_c}{\partial p} > 0$$
$$\frac{\partial r}{\partial t} = -M_c\frac{\partial r}{\partial p} \quad \text{otherwise} \tag{12}$$

where r_c is the saturation mixing ratio and α is computed to conserve moisture:

$$\alpha\sum_{k=l}^{l+n}(r_c - r)\left(\frac{\partial M_c}{\partial p}\right)^k = \sum_{k=l}^{l+n}M_c k\left(\frac{\partial r}{\partial p}\right)^k + \sum_{k=l}^{l+n}(\partial r)_c, \tag{13}$$

where it is assumed that convection occurs between layers l and $l + n$.

2.4.3. Kuo scheme. This scheme assumes that cumulus convection occurring in deep layers of unstable stratification is maintained by the moisture supply due to large-scale convergence and evaporation from the surface. It is also assumed that cumulus cloud air dissolves into the large-scale environment at the same rate as it is generated by the moisture supply. A large part of the moisture supplied into a cloud through its base and sides condenses during its ascent and either precipitates out or is stored as "cloud water." The precipitating portion is responsible for the net convective heating of the column, while the portion stored as cloud water is responsible for the moistening of the environment. This scheme was implemented following *Anthes* [1977].

Since the environment is modified through mixing of cumulus and environmental air, the cumulus convective heating and moistening are directly proportional to the local excess of cloud temperature and moisture over the corresponding environmental values. (The cloud temperature and moisture are computed by lifting a subcloud layer parcel pseudoadiabatically through the cloud layer, whose top is determined as the first level of neutral buoyancy of the lifted parcel.) The total moisture supply available for generating cumulus convection is assumed to be the total column large-scale convergence of moisture plus the amount supplied from below by surface evaporation. The moistening parameter b, of crucial importance for producing "realistic" heating rates, is specified by a method proposed by *Anthes* [1977] where the partitioning of convective heating and moistening is assumed to depend on the mean saturation deficit of the whole cloud layer:

$$b = \left(\frac{1 - \langle RH_{\text{env}}\rangle}{1 - RH_{\text{crit}}}\right)^n \quad \text{if } \langle RH_{\text{env}}\rangle > RH_{\text{crit}}$$
$$b = 1 \quad \text{otherwise} \tag{14}$$

where RH_{crit} is a threshold relative humidity below which only air moistening occurs, and

$$\langle RH_{\text{env}}\rangle = \frac{1}{p_{\text{base}} - p_{\text{top}}}\int_{p_{\text{base}}}^{p_{\text{top}}}\frac{r_{\text{env}}(p)\,dp}{r_{\text{sat}}(p, T_{\text{env}})}, \tag{15}$$

is the mean environmental relative humidity for the cloud layer and n and RH_{crit} are disposable parameters. According to *Kuo and Anthes* [1984], best results are obtained for values of n between 2 and 3 and RH_{crit} between 0.25 and 0.50. In our implementation we use values of $n = 2.5$ and $RH_{\text{crit}} = 0.35$.

After convection, large-scale saturation is checked at each layer. If necessary, large-scale condensation is activated following the procedure discussed by *Manabe et al.* [1965].

Left to its own devices, the Kuo scheme will eventually saturate a one-dimensional column and thus cannot be considered a true representation of an ensemble of convective clouds but only of convecting grid points. Thus as discussed for the SCA1.5D, to use the Kuo scheme in the framework of our radiative-convective equilibrium model, we calculate the vapor content of air outside of clouds and assume that the fractional area covered by clouds is small. This modified scheme is referred to as the Kuo1.5D scheme.

The convective mass flux is computed as in the SCA1.5D scheme, with the drying effect of the forced compensating subsidence now given by

$$\frac{\partial r}{\partial t} = -M_c\frac{\partial r}{\partial p}. \tag{16}$$

The detrainment of water is implicit in the Kuo scheme. The amount of moisture removed by the forced subsidence is added to the total supply of moisture, I. Therefore the supply of moisture used to perform the Kuo1.5D convective adjustment is

Table 1. Equilibrium Surface Temperatures, Evaporation Rates, and Values of the Sensible Heat Fluxes Obtained in Experiments With the HCA Scheme With Various Values of the Model's Arbitrary Parameters, as Indicated

Run	NL, levels	k_v, $m^2\ s^{-1}$	$C_D v_a$, ms^{-1}	Δt, s	T, °C	Evp, $mm\ d^{-1}$	F_θ, $W\ m^{-2}$
HSSTD	16	2.0	0.125	900	15.1	2.7	20
HS8L	8	···	···	···	15.8	2.6	15
HS32L	32	···	···	···	12.4	2.2	17
HS2KV	···	4.0	···	···	16.9	2.9	19
HS0KV	···	0.0	···	···	9.8	2.4	−121
HS2CD	···	···	0.250	···	14.7	3.6	4
HSDT2	···	···	···	1800	15.1	2.7	20

HCA, hard convective adjustment. NL, number of vertical layers.

$$I_{\text{dry}} = I + \sum_{k=l}^{l+n} \left(M_c \Delta t \frac{\partial r}{\partial p} \right)^k, \tag{17}$$

where Δt is the convective time step.

2.4.4. Goddard Institute for Space Studies (GISS) (1974) model 1 scheme. The GISS (1974) model 1 (GISS1) cumulus parameterization scheme is an adaptation of the three-level scheme proposed by *Arakawa* [1969]. Arakawa's scheme initiated a great deal of research attempting to parameterize cloud ensembles using a cloud spectrum and a simple cloud model. The *Arakawa* [1969] scheme is the first version of the widely known *Arakawa and Schubert* [1974] cumulus convection parameterization scheme. In the 1969 version, three types of convection can occur: middle-level convection, penetrative convection, and low-level convection. Each cloud type represents an ensemble of convective elements of small total area. Each cloud entrains environmental air through its base and through its sides and detrains cloud air at its upper level. The environment is modified by detrainment of moisture through the cloud top and compensating subsidence between the clouds. The latter both warms and dries the atmosphere.

Convection occurs whenever a nonentraining parcel of air rising pseudoadiabatically from the cloud base condenses and becomes positively buoyant by the time it reaches the cloud top layer. The closure assumption is that each cloud type will modify the environment, through detrainment and compensating subsidence, until $h^{\text{base}} = h^{\text{top}}_{\text{sat}}$, where h is the moist static energy and the subscript sat refers to the saturation value.

The contributions to the temperature and moisture, from all types of convection, are distributed in the model with strapped layers [*Somerville et al.*, 1974] and the large-scale condensation checked at each layer. Large-scale precipitation is assumed to occur whenever the specific humidity exceeds the saturation value, at any level. Condensation removes moisture and warms the atmosphere by releasing latent heat. The large-scale condensation adjustments are made following the procedure discussed by *Manabe et al.* [1965].

2.4.5. GISS model 2 (1983) scheme. This is the parameterization scheme used in the later GISS model 2 GCM [*Hansen et al.*, 1983]. This scheme, referred to as the GISS2 scheme, assumes that an undiluted plume is generated in moist convectively unstable layers and rises moist adiabatically up to its level of neutral buoyancy. The plume mass, M_c, is arbitrarily chosen as half the air mass of the cloud base grid-box. In our one-dimensional model we set the plume mass equal to 10% of the cloud base grid-box (this assumption better simulates the behavior of the 3-D model scheme). The environment is warmed and dried by the induced subsidence and moistened by the evaporation of falling precipitation. The falling precipitation is allowed to evaporate to the extent that it saturates half of the cloud area, defined as M_c/M_{a_k}, where M_{a_k} is the mass of layer k. Below cloud base, the falling precipitation is allowed to saturate the whole cloudy area. Large-scale condensation and dry adiabatic adjustment are computed by procedures similar to those used by *Manabe et al.* [1965].

2.4.6. Emanuel scheme. The main assumption in the scheme proposed by *Emanuel* [1991] is that the fundamental entities in cumulus convection are the sub-cloud-scale drafts rather than the cloud-scale circulations themselves. Convection occurs whenever the environment is unstable to a parcel in reversible adiabatic ascent from the surface. Vertical

Table 2. Equilibrium Surface Temperatures, Evaporation Rates, and Values of the Sensible Heat Fluxes Obtained in Experiments With the SCA1.5D Scheme With Various Model's Arbitrary Parameters

Run	NL, levels	k_v, $m^2\ s^{-1}$	$C_D v_a$, ms^{-1}	Δt, s	T, °C	Evp, $mm\ d^{-1}$	F_θ, $W\ m^{-2}$
SSSTD	16	2.0	0.125	900	15.2	2.6	19.5
SS32L	32	···	···	···	15.5	2.7	19.5
SS2CD	···	···	0.250	···	15.0	3.5	0.6
SSDT2	···	···	···	1800	15.2	2.7	19.0

Table 3. Equilibrium Surface Temperatures, Evaporation Rates, and Values of the Sensible Heat Fluxes Obtained in Experiments With the Kuol.5D Scheme With Various Model's Arbitrary Parameters

Run	NL, levels	k_v, $m^2 s^{-1}$	$C_D v_a$, ms^{-1}	Δt, s	T, °C	Evp, $mm\ d^{-1}$	F_θ, $W\ m^{-2}$
KSSTD	16	2.0	0.125	900	15.0	2.6	18.0
KS32L	32	...	...	...	14.4	3.2	8.2
KS2CD	...	...	0.250	...	14.9	3.6	1.9
KSDT2	...	...	...	1800	15.1	2.6	18.0

transports are accomplished by saturated updrafts and downdrafts, by a single unsaturated downdraft driven by evaporation of the falling precipitation, and by the compensating subsidence. The main closure parameters are the precipitation efficiencies of each saturated updraft, the fraction of the precipitation that falls through unsaturated air, and the rate of evaporation of falling precipitation. Dry adiabatic adjustment is performed before and large-scale condensation after moist convection, whenever necessary.

3. Sensitivity of the Climate Equilibria to the Model's Arbitrary Parameters

In this section we test the sensitivity of our radiative-convective equilibrium model to the various arbitrary parameters. We focus on the results of experiments with the HCA scheme. The HCA scheme is a simple and widely used [*Gates*, 1992] adjustment scheme with the highest sensitivity to changes in the arbitrary parameters among the schemes that we tested, and it represents a limiting case as the equilibrium troposphere is always saturated.

In the control run for the sensitivity experiment with the HCA scheme HSSTD (HCA sensitivity standard) (in Table 1) we adjust the solar forcing to obtain a surface equilibrium temperature near the global mean, 15°C, under clear sky conditions. The arbitrary parameters and their standard values are a drag coefficient, $C_D = 0.0025$; the wind speed at the anemometer level, $v_a = 5\ ms^{-1}$; the vertical diffusion coefficients for potential temperature and moisture, $k_{v\theta} = k_{vr} = k_v = 2\ m^2\ s^{-1}$; the number of vertical layers in the model's troposphere, NL = 16; and the mixed layer depth, 30 mbar. Above the troposphere there is a layer that reaches radiative equilibrium. In the experiments with 16 layers the potential temperature and the water vapor mixing ratio are assumed to be constant from the center of the lowest layer, at 970 mbar, down to the surface. However, in the experiments with higher and lower vertical resolutions the equivalent potential temperature and the relative humidity are assumed to be constant from the center of the lowest layer up or down to 970 mbar. From there the potential temperature and the water vapor mixing ratio are assumed to be constant, down to the surface. This is done to keep the mixed layer thickness constant in the resolution experiments.

Tables 1 through 6 present the sensitivity of the equilibrium surface temperature, the surface evaporation rate, and the surface sensible heat fluxes to some of the model's arbitrary parameters. The sensitivity of the radiative-convective equilibria to each of these parameters is discussed in the next sections.

3.1. Sensitivity With Respect to Vertical Resolution

In this subsection we discuss the sensitivity of the radiative-convective equilibrium to the model's vertical resolution. Experiments HS8L, HSSTD, and HS32L are for values of NL ranging from 8 to 32 levels with the HCA scheme and with fixed mixed layer depth.

Table 1 shows that for the experiments with the HCA scheme the equilibrium surface temperature is not very sensitive to changes in the vertical resolution (except for the high-resolution experiments, discussed below). The precipitation fields (not shown) for experiments HSSTD and HS8L reach a steady equilibrium, while the precipitation fields for experiment HS32L reach equilibrium only in a statistical sense. This occurs because increasing the vertical resolution decreases the numerical diffusion. Increasing the explicity diffusion eliminates this discrepancy, but reducing the time step does not. The temperature soundings through the model's atmosphere (not shown) closely follows a moist adiabat from the lowest level in all experiments, except in experiment HS32L. This happens because in experiment HS32L convection occurs only sporadically, since the saturation requirement is not always satisfied (due to the decrease in the intensity of the implicit numerical diffusion). The equi-

Table 4. Equilibrium Surface Temperatures, Evaporation Rates, and Values of the Sensible Heat Fluxes Obtained in Experiments With the GISS1 Scheme With Various Model's Arbitrary Parameters

Run	NL, levels	k_v, $m^2 s^{-1}$	$C_D v_a$, ms^{-1}	Δt, s	T, °C	Evp, $mm\ d^{-1}$	F_θ, $W\ m^{-2}$
G1SSTD	16	2.0	0.125	900	14.9	3.2	2.0
G1S8L	8	...	...	...	13.3	3.3	−6.5
G1S2CD	...	...	0.250	...	15.2	3.5	−1.2
G1SDT2	...	...	...	1800	14.9	3.2	2.0

Table 5. Equilibrium Surface Temperatures, Evaporation Rates, and Values of the Sensible Heat Fluxes Obtained in Experiments With the GISS2 Scheme With Various Model's Arbitrary Parameters

Run	NL, levels	k_v, $m^2\ s^{-1}$	$C_D v_a$, ms^{-1}	Δt, s	T, °C	Evp, $mm\ d^{-1}$	F_θ, $W\ m^{-2}$
G2SSTD	16	2.0	0.125	900	15.3	3.3	2.5
G2S32L	32	...	...	...	16.8	3.5	5.4
G2S2CD	...	...	0.250	...	15.2	4.1	−12.6
G2SDT2	...	...	...	1800	15.3	3.3	2.5

librium atmosphere is saturated in all resolution experiments, except in experiment HS32L.

Tables 2 through 6 show that the surface temperatures and evaporation rates obtained in the experiments with the SCA1.5D, Kuo1.5D, GISS1, GISS2, and Emanuel schemes are, in general, not very sensitive to the vertical resolution but the surface sensible heat fluxes are. However, Table 6 shows that the Emanuel scheme requires reasonably high resolution (16 layers) to be accurate. Also, the temperature and the relative humidity soundings (not shown) obtained in experiments with the Emanuel scheme show a tendency for the relative humidity and convective available potential energy (CAPE) to increase as the resolution decreases, probably because of restrictions on the mixing events. Because the GISS1 scheme is a three-layer scheme, we restrict the resolution to less than 16 layers in our resolution experiments with it.

The optimal vertical resolution is the one which offers the best compromise between central process unit (CPU) time per experiment and reasonable physical behavior of the model. For this reason we choose 16 layers in the model's troposphere (the total number of layers is 26, 10 layers being in the model's stratosphere) as the standard value to be used throughout this paper and parts 2 and 3. Although this may not be high enough for good resolution in some cases (e.g., GISS2 and Emanuel schemes), it is still higher than those used in most climate studies with GCMs [*Boer et al.*, 1992; *Gates*, 1992].

3.2. Sensitivity With Respect to Diffusion

In this subsection we discuss briefly the sensitivity of the radiative-convective equilibria to the value of the Fickian diffusion coefficient. Experiments HS0KV and HS2KV, in Table 1, show the results of two experiments with the HCA scheme, one in which the diffusion coefficient is set to zero and another in which it is set to twice the value used in the standard experiment (experiment HSSTD).

In the experiments with the HCA scheme, doubling the value of K_v leads to an increase of 1.8°C in the surface temperature and of 0.2 $mm\ d^{-1}$ in the surface evaporation as well as a decrease of 1.0 $W\ m^{-2}$ in the surface sensible heat fluxes. The increase in the surface temperature is due to an increase of the greenhouse effect resulting from an increase in the water vapor mixing ratio of the troposphere (of about 13% at the lowest level). Setting the diffusion coefficient to zero leads to a decrease of 5.3°C in the surface temperature, of 0.3 $mm\ d^{-1}$ in the surface evaporation, and of 141 $W\ m^{-2}$ in the surface sensible heat fluxes. Furthermore, the precipitation field (not shown) becomes unsteady and large-scale condensation occurs in all levels between 370 mbar and the surface. The average atmosphere is no longer moist neutral to parcel ascent from the boundary layer. The decrease in the surface temperature is due to a decrease in the greenhouse effect (the equilibrium atmosphere is no longer saturated). The unsteadiness of the convective adjustments and, consequently, of the precipitation field is related to the fact that CAPE is present in the equilibrium atmosphere. When the saturation criteria are satisfied, a large adjustment occurs. We do not present results of sensitivity studies to the Fickian diffusion coefficient for the other cumulus schemes.

3.3. Sensitivity With Respect to the Bulk Aerodynamic Parameter

The bulk aerodynamic formula parameter, $C_D v_a$, controls evaporation and sensible heat fluxes at the surface. Throughout this series of papers, unless otherwise specified, we assume it to be 0.0125 $m\ s^{-1}$ which corresponds to an anemometer level velocity of 5 $m\ s^{-1}$ and an aerodynamic drag coefficient of 0.0025.

The results of experiment HS2CD with the HCA scheme,

Table 6. Equilibrium Surface Temperatures, Evaporation Rates, and Values of the Sensible Heat Fluxes Obtained in Experiments With the Emanuel Scheme With Various Model's Arbitrary Parameters

Run	NL, levels	k_v, $m^2\ s^{-1}$	$C_D v_a$, ms^{-1}	Δt, s	T, °C	Evp, $mm\ d^{-1}$	F_θ, $W\ m^{-2}$
ESSTD	16	2.0	0.125	900	15.2	3.2	7.4
ES8L	8	...	...	...	20.3	3.4	4.9
ES32L	32	...	...	...	13.6	3.1	9.3
ES2KV	...	4.0	...	...	16.9	3.5	5.6
ES2CD	...	...	0.250	...	15.0	3.8	−2.3
ESDT2	...	...	...	1800	15.3	3.2	7.7

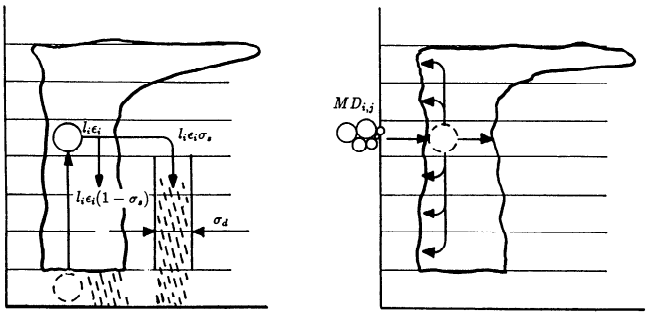

Figure 1. Schematic diagram showing the microphysical parameters of the Emanuel scheme.

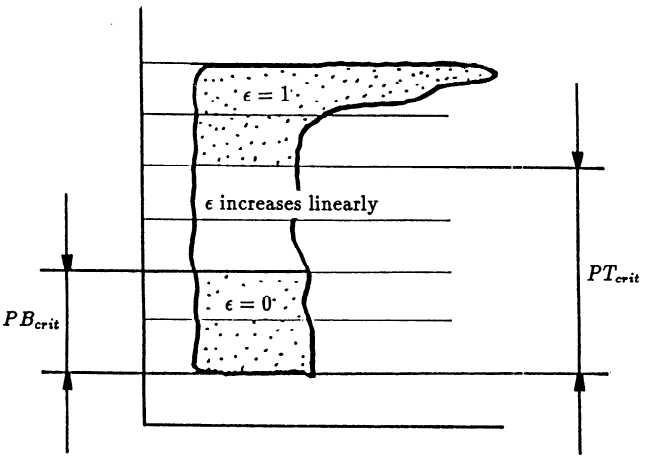

Figure 2. Schematic diagram showing the precipitation efficiency parameter of the Emanuel scheme.

displayed in Table 1, show that the $C_D v_a$ parameter controls the partition among surface infrared radiative flux, evaporation, and the surface sensible heat fluxes without drastically changing the surface equilibrium temperature. Doubling $C_D v_a$ leads to a decrease of 0.4°C in the surface temperature and of 16.0 W m^{-2} in the surface sensible heat fluxes, as well as to an increase of 0.9 mm d^{-1} in the surface evaporation. This is due to changes in the temperature and moisture discontinuities at the surface which, in turn, causes changes in the net infrared radiation flux at the surface.

Experiments SS2CD, KS2CD, G1S2CD, G2S2CD, and ES2CD (see Tables 2–6) show the results of experiments with the SCA1.5D, Kuo1.5D, GISS1, GISS2, and Emanuel schemes, respectively, in which the $C_D v_a$ parameter is twice the value used in the standard experiments. They also show that in general, there is a small decrease in the equilibrium surface temperature (except in the experiment with the GISS1 scheme, where there is a small increase, probably because of arbitrary changes in the strapping of the layers into the three "convective layers"), an increase in the evaporation rates, and a decrease in the surface sensible heat fluxes.

3.4. Sensitivity With Respect to the Time Step

The results of experiments in which the time step was halved, experiments HSDT2, SSDT2, KSDT2, G1SDT2, G2SDT2, and ESDT2 are displayed in Tables 2–6. They show that the various schemes are not sensitive to the time step. Halving the time step, in relation to our standard value of 15 min, in general produces imperceptible changes in the equilibrium state.

4. Sensitivity of Climate Equilibria to Cloud Microphysical Parameters

In this section we use the *Emanuel* [1991] cumulus convection scheme to test the sensitivity of climate simulations to the parameterization of cloud microphysical processes. In the Emanuel scheme the moistening of the atmosphere is parameterized on the basis of cloud microphysical processes. The "microphysical parameters" of this scheme are the precipitation efficiencies, ε_i, describing the fraction of condensed water converted to precipitation in each of i sub-cloud-scale updrafts; the fractional area covered by the precipitating downdraft, σ_d; and the fraction of precipitation that falls through unsaturated environment, σ_{s_i}. We tested the sensitivity of the radiative-convective equilibria obtained with the Emanuel scheme to these "microphysical parameters." The physical meaning of these parameters is schematically illustrated in Figures 1 and 2.

4.1. Equilibrium Surface Temperature

Tables 7 and 8 display the equilibrium surface (swamp) temperatures obtained in experiments with the Emanuel cumulus convection scheme with various microphysical parameters. The results presented in Table 7 are for vertically varying precipitation efficiencies, and the results presented in Table 8 are for constant precipitation efficiencies (throughout the convecting layers). PB_{crit} and PT_{crit} are, respectively, the critical draft thicknesses below which the precipitation efficiencies, ε_i, are assumed to be zero and above which they are taken to be the unity. The precipitation efficiencies throughout the convecting layers are arbitrarily computed as follows:

$$\begin{aligned} \varepsilon_i &= 0, && p_{icb} - p_i < PB_{crit} \\ \varepsilon_i &= \frac{p_{icb} - p_i - PB_{crit}}{PT_{crit} - PB_{crit}}, && PB_{crit} < p_{icb} - p_i < PT_{crit} \\ \varepsilon_i &= 1, && p_{icb} - p_i > PT_{crit}, \end{aligned} \tag{18}$$

where p_{icb} is the cloud base pressure level; σ_d and σ_s are the fractional areas covered by unsaturated downdraft and the

Table 7. Equilibrium Surface ("Swamp") Temperatures Obtained in Experiments With the Emanuel Cumulus Convection Scheme With Various Microphysical Parameters

	Cloud Microphysical Parameters				
Run	PB_{crit}, mbar	PT_{crit}, mbar	σ_d	σ_s	T, °C
STD	150	500	0.010	0.150	26.0
LGE	···	200	···	···	22.4
LWE	···	700	···	···	29.8
ELE	···	800	···	···	runway
LSD	···	···	0.100	···	29.8
SSS	···	···	···	0.015	22.9

Table 8. Same as Table 7 Except for the Precipitation Efficiencies, ε_i, That Now Are Constant Throughout the Clouds

Run	Cloud Microphysical Parameters			
	ε_i	σ_d	σ_s	T, °C
HCE	1.0	0.010	0.150	22.0
LCE	0.1	...	...	runway

fraction of precipitation falling outside clouds, respectively. The solar forcing is set at 342.9 W m^{-2} and the surface albedo at 0.102. Clear sky conditions are used in the computation of the radiative fluxes.

The results presented in Tables 7 and 8 clearly indicate that the equilibrium temperature can be very sensitive to cloud microphysics. In section 4.2 we analyze the reasons for this high sensitivity as well as the effects of the changes of the microphysical parameters on the convective and radiative processes and on the equilibrium atmosphere.

4.2. Equilibrium Atmospheres

Figure 3 display the characteristics of the equilibrium atmosphere for an experiment with the set of standard parameters. These standard parameters are indicated on the first row of Table 7, experiment STD. The model is tuned to produce a surface equilibrium temperature of 26°C, typical of tropical regions. The precipitation and sensible heat flux fields (not shown) reach a steady equilibrium (after a few hundred days). The equilibrium precipitation is about 4.9 mm d^{-1}, equal to the evaporation, and the surface latent heat flux is about 142 W m^{-2}. The equilibrium sensible heat flux is about 2 W m^{-2}, very small (1.4%) when compared to the latent heat flux.

The temperature tendencies, averaged over the last 10 days of integration (not displayed) show that in the interior of the troposphere the net radiative cooling (about −1.5 K d^{-1}) is nearly balanced by the net convective heating (since the diffusive heat fluxes convergence is small). The boundary layer is cooled by radiation (about −2.5 K d^{-1}) and warmed both by convection (about 0.5 K d^{-1}) and surface sensible heat flux (about 2.0 K d^{-1}). The diffusive heat flux convergence is weak in the interior of the troposphere (less than 0.2 K d^{-1}). It is stronger (about 0.4 K d^{-1}) at the upper troposphere, where there is a sharp increase in potential temperature (to match the tropopause temperature). Large-scale condensation is not present when equilibrium is reached.

The water vapor mixing ratio tendencies, averaged over the last 10 days of integration (not displayed), show that the net convective moistening is very small in the interior of the troposphere. The drying by forced subsidence is balanced by the moistening resulting from detrainment of cloud air and evaporation of precipitation. Diffusive moisture fluxes are very weak in the interior. In the boundary layer, convective drying balances evaporation. As mentioned above, large-scale condensation is not present when equilibrium is reached.

Figure 3 displays soundings through the model's atmosphere averaged over 10 days, at the end of the integration. The atmosphere is always saturated at the tropopause, because that is the level at which saturated cloud air is detraining.

A buoyancy sounding (at the end of the integration, averaged over 10 days) is presented in Figure 4. The temperature departures from the pseudoadiabat are mostly smaller than 2°C. It is important to remember that the Emanuel scheme relaxes the environment temperature toward a reversible virtual moist adiabat (smaller temperatures at lower levels and larger at upper levels).

In the large precipitation efficiency (LGE) experiment, row 2 in Table 7, we increase the precipitation efficiency, ε_i, by decreasing the updraft depth above which $\varepsilon_i = 1.0$, i.e., by decreasing PT_{crit} from 500 to 200 mbar. Here, the precipitation field (not shown) is unsteady, reaching a statistical equilibrium after a few hundred days. The equilibrium precipitation is about 4.4 mm d^{-1}, equal to the evaporation with the latent heat flux at about 128 W m^{-2}. The equilibrium sensible heat flux is around 7 W m^{-2}. The Bowen ratio ($b = C_p F_T / L_v F_q$) is now increased from 0.014, in experiment STD, to 0.055. For reference, over the undisturbed tropical ocean, b is equal to about 0.07 [*Pond et al.*, 1971].

Temperature tendencies, averaged over the last 10 days of

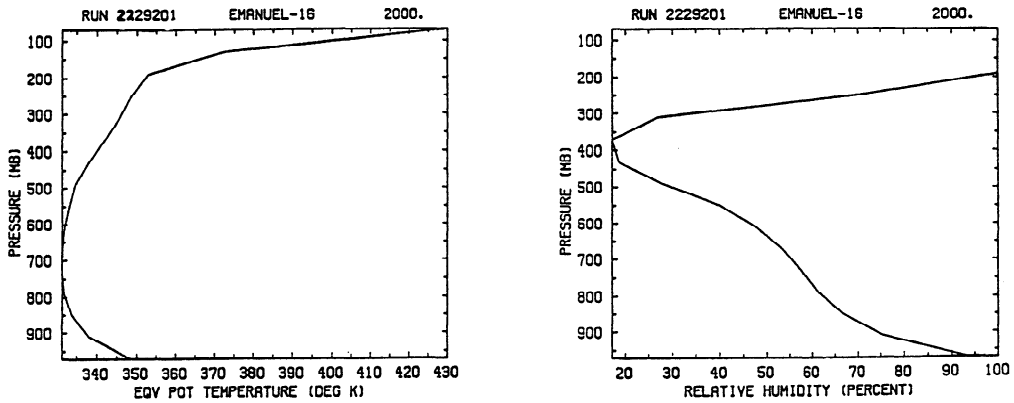

Figure 3. Vertical soundings throughout the model's atmosphere, averaged over the last 10 days of integration (960 time steps). (a) Equivalent potential temperature. (b) Relative humidity. The STD (standard run) set of parameters are used in this experiment.

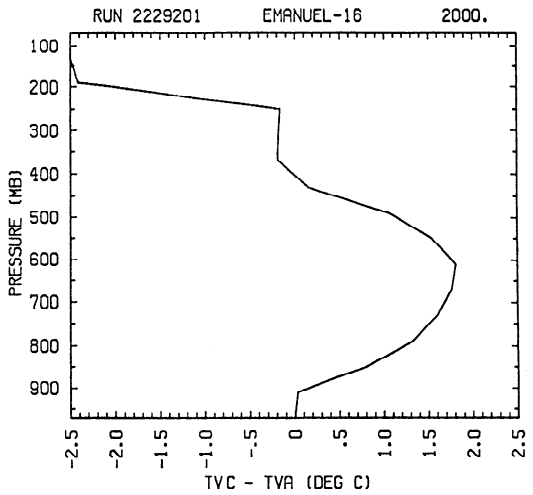

Figure 4. The difference between the virtual temperature of pseudoadiabatically lifted surface air and environmental virtual temperature, averaged over the last 10 days of integration. The STD set of parameters are used in this experiment.

integration (not displayed) show that the net radiative cooling is substantially reduced in the upper troposphere and increased in the boundary layer. This occurs because the water vapor mixing ratio throughout the troposphere is now smaller than the one obtained in the standard run (due to a decrease in temperature and relative humidity). Diffusive flux convergences are stronger in the interior of the troposphere (by about 0.2 K d^{-1}) due to a less smooth distribution of moistening by convection (resulting from the stronger precipitation efficiency gradient). Again, there is no large-scale condensation when equilibrium is reached. In the boundary layer a smaller convective drying balances a smaller evaporation, when compared to the STD experiment. A weak diffusive moisture flux moistens the interior troposphere, from 790 to 550 mbar. This moistening is compensated by convective subsidence drying.

When compared with the STD experiment, the sounding throughout the model's atmosphere (Figure 5) shows a sharper minimum θ_e peak at around 700 mbar and a smaller, lower, and broader *RH* minimum at the middle troposphere. It also displays a stronger decrease in *RH* from the boundary layer to the middle troposphere and higher *RH* in the upper troposphere.

Figure 6 displays the characteristics of the equilibrium atmosphere for the low precipitation efficiency (LWE) experiment, as indicated in Table 7. In this experiment the precipitation and sensible heat flux fields, not displayed, reach a steady equilibrium over a period of a few hundred days. Now, the equilibrium precipitation is about 5.5 mm d^{-1} and is equal to the evaporation, with the latent heat flux, at about 159 W m^{-2}. The equilibrium sensible heat flux is about 1.5 W m^{-2}, very small when compared to the latent heat flux. The Bowen ratio, *b*, is 0.009, a lower value when compared with the standard run (STD experiment). A decrease in the precipitation efficiency results in a decrease of the Bowen ratio.

When compared with the STD experiment, the net radiative cooling (not shown) is increased in the upper troposphere and decreased in the boundary layer. This occurs because the water vapor content throughout the troposphere (see Figure 6) is now higher (low precipitation efficient clouds detrain more moisture into the environment) than the one obtained in the standard run (due to a increase in temperature and relative humidity, mostly between 900 and 450 mbar). The diffusive fluxes of temperature (not shown) are a little weaker in the boundary layer, due to the smaller sensible heat flux. Diffusive fluxes of moisture vanish above 670 mbar. Below this level, diffusive moistening is compensated by convective drying. In the boundary layer a stronger convective drying balances a stronger evaporation, when compared to the STD experiment. Again, there is no large-scale condensation when equilibrium is reached.

In the LWE experiment the model's atmosphere is warmer and moister than that of the STD experiment. Figure 6 shows that the *RH* is larger throughout the model's troposphere. The larger *RH* induces a stronger greenhouse feedback, that, in turn, produces a warmer troposphere. The larger increase in *RH* occurs in the middle troposphere, where the penetrative downdraft mass flux (not shown) is maximum. The decrease in precipitation efficiency produces an increase in the penetrative downdraft mass flux, which, in turn, increases the moistening of the middle troposphere.

The extra low precipitation efficiency (ELE) experiment produces excessive detrainment of water vapor, which results in a very moist atmosphere. Equilibrium is no longer possible; the strong water vapor feedback produces a run-

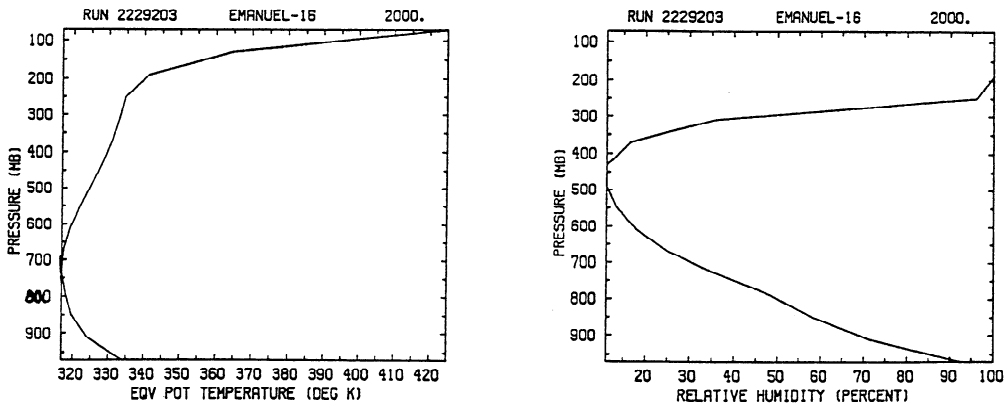

Figure 5. As in Figure 3 but for the large precipitation efficiency experiment.

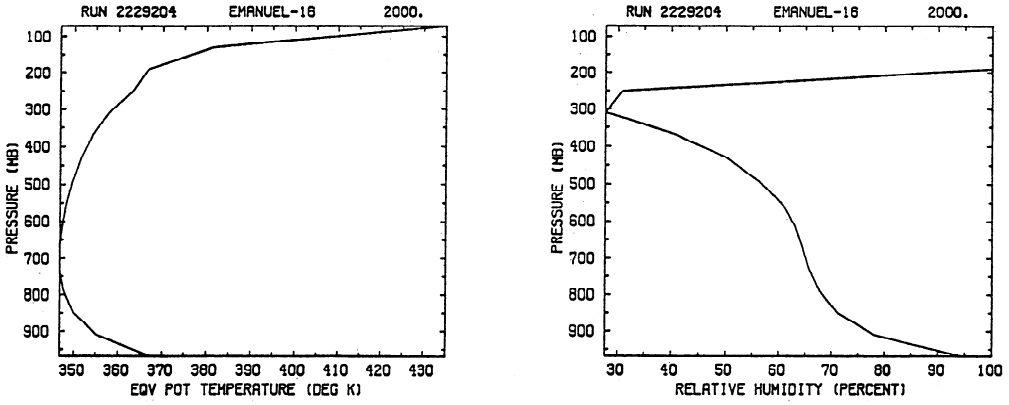

Figure 6. As in Figure 3 but for the low precipitation efficiency experiment.

away greenhouse. The runaway greenhouse is discussed in detail in another paper (part 2).

In the large sigma-D (LSD) experiment (or large area covered by unsaturated downdrafts) the area covered by unsaturated downdrafts is increased by a factor of 10 in relation to the STD experiment. Results of this experiment are shown in Figure 7 and Table 7.

The precipitation and sensible heat flux fields (not shown) reach a steady equilibrium over a period of a few hundred days. Now, the equilibrium precipitation is about 5.3 mm d^{-1}, equal to the evaporation, with the latent heat flux, at about 155 W m^{-2}. The equilibrium sensible heat flux is about 8 W m^{-2}, and the Bowen ratio, b, is equal to 0.052, an increased value, when compared with that obtained in the STD experiment. Therefore an increase in the area covered by unsaturated downdrafts results in further increases in the Bowen ratio.

Since the water vapor content throughout the troposphere (Figure 7) is higher in relation to the STD experiment, the net radiative cooling (not shown) is increased in the upper troposphere and decreased in the boundary layer. The increase in moistening occurs because, now, the falling precipitation is able to increase the moisture content of a larger fractional area. The increase in evaporation of falling precipitation generates a more intense unsaturated downdraft, that, in turn, produces a stronger cooling of the boundary layer. The diffusive flux of temperature is a little stronger in the boundary layer due to the larger sensible heat flux. Diffusive fluxes of moisture are also slightly stronger, especially in the boundary layer (since surface evaporation is more intense). The stronger radiative cooling of the upper troposphere drives a larger convective mass flux. Consequently, more moisture is detrained at the level of neutral buoyancy. Then, supersaturation occurs, and large-scale condensation removes it.

In the LSD experiment the model's atmosphere is warmer and wetter below 370 mbar and drier above 310 mbar (Figure 7). As mentioned before, the wetter middle-lower troposphere is due to the increased evaporation in the unsaturated downdraft, while the drier upper troposphere is due to increased drying by the larger compensating subsidence (necessary to balance the stronger radiative cooling at those levels). As observed in the experiments with smaller precipitation efficiency, the larger RH induces a stronger greenhouse feedback, than, in turn, produces a warmer troposphere (larger θ in Figure 7). The larger increase in RH occurs in the lower troposphere, where the unsaturated downdraft mass flux (not shown) is maximum.

In the small sigma-S (SSS) experiment (or small fraction of precipitation falling through unsaturated environment), the fraction of precipitation falling through unsaturated environment is decreased by a factor of 10 in relation to the STD experiment. The precipitation and sensible heat flux fields (not shown) reach a steady equilibrium over a period of a few hundred days. Now, the equilibrium precipitation is about 4.1 mm d^{-1}, equal to the evaporation, with the latent heat flux, at about 119 W m^{-2}. The equilibrium sensible heat flux

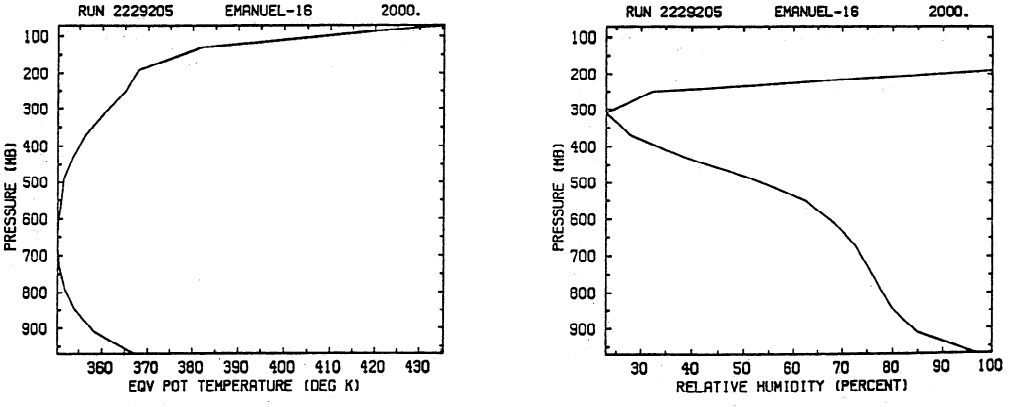

Figure 7. As in Figure 3 but for the large sigma-D experiment.

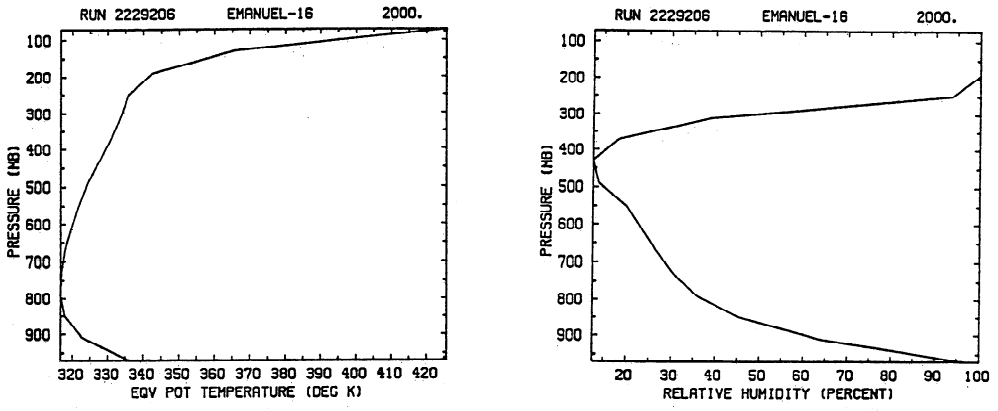

Figure 8. As in Figure 3 but for the small sigma-S experiment.

is about 11 W m^{-2}, and the Bowen ratio, b, is 0.092, an increased value when compared with that obtained in the standard run. The surface sensible heat flux increases to balance the stronger radiative cooling of the boundary layer. Therefore a decrease in the fraction of precipitation falling outside of clouds increases the Bowen ratio.

Since the water vapor mixing ratio throughout the troposphere (Figure 8) is lower in relation to the STD experiment, the net radiative cooling (not shown) is decreased in the upper troposphere and increased in the boundary layer. This decrease in moisture occurs because, now, only a small fraction of the falling precipitation is allowed to evaporate. The decrease in the moistening by the unsaturated downdraft produces a drier middle-lower troposphere, which, in turn, induces a stronger radiative cooling of the boundary layer. Compared to the STD experiment, the diffusive flux of temperature is 33% stronger in the boundary layer (due to the larger sensible heat flux) and the diffusive flux of moisture is 36% weaker (since surface evaporation is less intense). Large-scale condensation does not occur at equilibrium. In the SSS experiment the equilibrium atmosphere is colder and drier (Figure 8), except above 370 mbar, where the SSS experiment produces a higher RH.

5. Summary and Conclusions

The hydrological cycle is explicitly included in a one-dimensional radiative-convective equilibrium model which is coupled to a swamp surface and tested with various cumulus convection schemes. The essential difference between this and other radiative-convective models lies in the explicit computation of the atmosphere's water vapor profile. In our model the moisture profile is interactively computed by the cumulus convection scheme. This has a crucial influence on the computation of the radiative fluxes throughout the atmosphere and therefore on the model's sensitivities.

We analyzed the sensitivities of this radiative-convective model to changes in the values of its arbitrary parameters and on the cloud microphysical parameters. The results of experiments with the HCA scheme represents an upper bound on the sensitivity of the radiative-convective equilibria, because it commonly saturates the atmosphere. Results of experiments with the other cumulus convection schemes (which produce a more realistic RH vertical profile), or of experiments in which the RH profile is fixed (based on climatological values), in general, did show relatively very small sensitivities to changes in the model's arbitrary parameters.

For values of the total diffusion (numerical and explicit) above a minimum value sufficient to keep the atmosphere saturated, the equilibrium state obtained with the HCA scheme is steady and not very sensitive to increases in the diffusion coefficient. However, for values of the diffusion coefficient below this minimum, the saturation criteria for HCA to occur are only rarely satisfied. Then, CAPE builds up and the equilibrium is stochastic. The HCA breaks down, because of its inability to produce an efficient vertical transport of water substance ("large-scale" condensation occurs in the lowest layer). We also show that the equilibrium surface temperature is not very sensitive to changes in the bulk aerodynamic parameter and to the time step. But since the bulk aerodynamic parameter controls the temperature discontinuity at the surface, which in turn produces changes in the net infrared radiation flux at this level, the surface sensible heat fluxes and evaporation rates are sensitive to its value.

Using the *Emanuel* [1991] scheme, we show that the climate equilibrium depends crucially on cloud microphysical processes. Clouds with high precipitation efficiency produce cold and dry climates. This happens because most of the cloud-condensed water falls out as rain, leaving little available to moisten the atmosphere. Clouds with low precipitation efficiency lead to moist and warm climates. The large moisture content is due to the fact that these clouds detrain large amounts of water substance into the environment. The strong greenhouse effect of this very moist atmosphere produces high equilibrium temperatures.

Since climate equilibrium can be very sensitive to the cloud microphysical processes, any cumulus convection scheme adequate for use in GCMs should be strongly based on them. Considering that the cumulus convection schemes currently in use in GCMs are based on somewhat arbitrary moistening assumptions, they are probably inadequate for climate change studies. It is difficult to imagine that complex cloud microphysical processes will ever be represented adequately in GCMs. Thus it is extremely important to devise tests of cumulus representations which assess their ability to predict atmospheric water vapor. A commonly used method involves the comparison of heating and moistening profiles produced by convection schemes with those diagnosed from arrays of soundings, such as the one de-

ployed during the Global Atlantic Tropical Experiment (GATE). There are two major drawbacks to this approach. First, small differences between observed and predicted moistening may lead to substantial changes in humidity, if they persist even for a relatively short time. Second, small differences may result from the initial relaxation of the atmosphere to the model's natural equilibrium state, independently of how good the convection scheme is. Therefore a different approach is called for. We recommend the use of time series of horizontal advection of heat and water vapor, vertical motion, surface fluxes, and radiative heating, derived from rawindsonde networks (such as the one used in GATE), in conjunction with several cumulus schemes to make predictions of the evolution, with time, of the vertical profiles of equivalent potential temperature and relative humidity. These are very sensitive predictands.

No verification scheme can assess the ability of convective representations to predict humidity in the upper troposphere for the simple reason that good measurements are not currently available (rawindsonde measurements are not reliable in the upper troposphere and satellite measurements are still very limited). This is a major problem, as small changes in humidity at high altitudes have a strong effect on radiative transfer.

Acknowledgments. We would like to thank M.-D. Chou and W. Ridgway of NASA Goddard Space Flight Center for providing us with the radiation code and for promptly answering our numerous questions.

References

Anthes, R. A., A cumulus parameterization scheme utilizing a one-dimensional cloud model, *Mon. Weather Rev.*, *105*, 270–300, 1977.

Arakawa, A., Parameterization of cumulus convection, in *Proceedings of the WMO/IUGG Symposium of Numerical Weather Prediction*, pp. 1–6, Japan Meteorological Society, Tokyo, 1969.

Arakawa, A., and W. H. Schubert, Interaction of a cumulus cloud ensemble with the large-scale environment, I, *J. Atmos. Sci.*, *31*, 674–701, 1974.

Asselin, R., Frequency filter for time integrations, *Mon. Weather Rev.*, *100*, 437–490, 1972.

Betts, A. K., Saturation point analysis of moist convective overturning, *J. Atmos. Sci.*, *39*, 1484–1505, 1982.

Betts, A. K., Mixing line analysis of clouds and cloudy boundary layers, *J. Atmos. Sci.*, *42*, 2751–2763, 1985.

Betts, A. K., and W. Ridgway, Coupling of the radiative, convective, and surface fluxes over the equatorial Pacific, *J. Atmos. Sci.*, *45*, 522–536, 1988.

Betts, A. K., and W. Ridgway, Climatic equilibrium of the atmospheric convective boundary layer over a tropical ocean, *J. Atmos. Sci.*, *46*, 2621–2641, 1989.

Boer, G. J., et al., Some results from an intercomparison of the climates simulated by 14 atmospheric general circulation models, *J. Geophys. Res.*, *97*, 12,771–12,786, 1992.

Cess, R. D., et al., Intercomparison and interpretation of climate feedback processes in 19 atmospheric general circulation models, *J. Geophys. Res.*, *95*, 16,601–16,615, 1990.

Chou, M.-D., Broadband water vapor transmission functions for atmospheric IR flux computations, *J. Atmos. Sci.*, *41*, 1775–1778, 1984.

Chou, M.-D., A solar radiation model for use in climate studies, *J. Atmos. Sci.*, *49*, 762–772, 1992.

Chou, M.-D., and L. Kouvaris, Monocromatic calculations of atmospheric radiative transfer due to molecular line absorption, *J. Geophys. Res.*, *91*, 4047–4055, 1986.

Chou, M.-D., and L. Peng, A parameterization of the absorption in the 15 μm CO_2 spectral region with application to climate sensitivity studies, *J. Atmos. Sci.*, *40*, 2183–2192, 1983.

Chou, M.-D., D. P. Krats, and W. Ridgway, Infrared radiation parameterization in numerical climate models, *J. Clim.*, *4*, 424–437, 1991.

Emanuel, K. A., A scheme for representing cumulus convection in large-scale models, *J. Atmos. Sci.*, *48*, 2313–2335, 1991.

Gates, W. L., AMIP: The Atmospheric Model Intercomparison Project, *Bull. Am. Meteorol. Soc.*, *73*, 1962–1970, 1992.

Hansen, J., G. Russell, D. Rind, P. Stone, A. Lacis, S. Lebedeff, R. Ruedy, and L. Travis, Efficient three-dimensional global models for climate studies: Model I and II, *Mon. Weather Rev.*, *111*, 609–662, 1983.

Krishnamurti, T. N., Y. Ramanathan, H. Pan, R. J. Pasch, and J. Molonari, Cumulus parameterization and rainfall rates, I, *Mon. Weather Rev.*, *108*, 465–472, 1980.

Kuo, H. L., Further studies of the parameterization of the influence of cumulus convection on large-scale flow, *J. Atmos. Sci.*, *31*, 1232–1240, 1974.

Kuo, H. L., and R. A. Anthes, Semi-prognostic tests of Kuo-type cumulus parameterization schemes in an extratropical convective system, *Mon. Weather Rev.*, *112*, 1498–1509, 1984.

Lindzen, R. S., Some remarks on cumulus parameterization, *Pure Appl. Geophys.*, *126*, 123–135, 1988.

Lindzen, R. S., Some coolness concerning global warming, *Bull. Am. Meteorol. Soc.*, *71*, 288–299, 1990.

Lindzen, R. S., A. Y. Hou, and B. F. Farrel, The role of convective model choice in calculating the climate impact of doubling CO_2, *J. Atmos. Sci.*, *39*, 1189–1205, 1982.

Manabe, S., Estimate of future changes of climate due to man's increase of carbon dioxide concentration in the air, in *Man's Impact on Climate*, edited by W. H. Mattews, W. W. Kellogg, and G. D. Robinson, 594 pp., MIT Press, Cambridge, Mass., 1971.

Manabe, S., and R. F. Strickler, Thermal equilibrium of the atmosphere with a convective adjustment, *J. Atmos. Sci.*, *21*, 361–385, 1964.

Manabe, S., and R. T. Wetherald, Thermal equilibrium of the atmosphere with a given distribution of relative humidity, *J. Atmos. Sci.*, *24*, 241–259, 1967.

Manabe, S., J. Smagorinsky, and R. F. Strickler, Simulated climatology of a general circulation model with a hydrologic cycle, *Mon. Weather Rev.*, *93*, 769–798, 1965.

Manabe, S., R. J. Stouffer, M. J. Spelman, and K. Bryan, Transient response of a coupled ocean-atmosphere model to gradual changes of atmospheric CO_2, I, Annual mean response, *J. Clim.*, *4*, 785–819, 1991.

McClatchey, R. A., R. W. Fenn, J. E. A. Selby, F. E. Volz, and J. S. Garing, Optical properties of the atmosphere, *Environ. Res. Pap.*, *411*, Air Force Cambridge Res. Labs., 1972.

Pond, S., G. T. Phelps, and J. E. Paquin, Measurements of the turbulent fluxes of momentum, moisture, and sensible heat over the ocean, *J. Atmos. Sci.*, *28*, 901–928, 1971.

Rennó, N. O., Cumulus convection parameterization and numerical modelling of moist atmospheres, Ph.D. thesis, 297 pp., Mass. Inst. of Technol., Cambridge, 1992.

Sarachik, E. S., Tropical sea surface temperature: An interactive one-dimensional atmosphere ocean model, *Dyn. Atmos. Oceans*, *2*, 455–469, 1978.

Sarachik, E. S., A simple theory for the vertical structure of the tropical atmosphere, *Pure Appl. Geophys.*, *123*, 261–269, 1985.

Somerville, R. C. J., P. H. Stone, M. Harlen, J. E. Hansen, J. S. Hogan, L. M. Druyan, G. Russell, A. A. Lacis, W. J. Quirk, and J. Tenenbaum, The GISS model of the global atmosphere, *J. Atmos. Sci.*, *31*, 84–117, 1974.

Stone, P. H., and J. Risbey, On the limitations of general circulation climate models, *Geophys. Res. Lett.*, *17*, 2173–2176, 1990.

Wang, W.-C., and P. H. Stone, Effect of ice-albedo feedback on global sensitivity in a one-dimensional radiative-convective climate model, *J. Atmos. Sci.*, *37*, 545–552, 1980.

K. E. Emanuel, Center for Meteorology and Physical Oceanography, Massachusetts Institute of Technology, Cambridge, MA 02139.

N. O. Rennó, Lawrence Livermore National Laboratory, Mail Code L262, P.O. Box 808, Livermore, CA 94551.

(Received March 10, 1993; revised December 7, 1993; accepted December 27, 1993.)